GLOBAL BIOGEOCHEMICAL CYCLES, VOL. 27, 1–13, doi:10.1002/gbc.20058, 2013

The influence of net community production and phytoplankton community structure on CO_2 uptake in the Gulf of Alaska

Hilary I. Palevsky,[1] Francois Ribalet,[1] Jarred E. Swalwell,[1] Catherine E. Cosca,[2] Edward D. Cokelet,[2] Richard A. Feely,[2] E. Virginia Armbrust,[1] and Paul D. Quay [1]

Received 16 October 2012; revised 24 April 2013; accepted 21 June 2013.

[1] Biological productivity is a key factor controlling the ocean's ability to take up carbon dioxide from the atmosphere. However, the ecological dynamics that drive regions of intense productivity and carbon export are poorly understood. In this study, we present high-spatial-resolution estimates of air-sea CO_2 flux, net community production (NCP) rates calculated from O_2/Ar ratios, and phytoplankton population abundances determined by continuous underway measurements on a cruise across the Gulf of Alaska in May 2010. The highest rates of NCP (249 ± 40 mmol C m^{-2} d^{-1}) and oceanic CO_2 uptake (air-sea flux of -42.3 ± 6.1 mmol C m^{-2} d^{-1}) were observed across a transition zone between the high-nitrate low-chlorophyll (HNLC) waters of the Alaskan Gyre and the coastal waters off the Aleutian Islands. While the transition zone comprises 20% of the total area covered in crossing the Gulf of Alaska, it contributed 58% of the total NCP and 67% of the total CO_2 uptake observed along the cruise track. A corresponding transition zone phytoplankton bloom was dominated by two small-celled (<20 μm) phytoplankton communities, which were distinct from the phytoplankton communities in the surrounding Alaskan Gyre and coastal waters. We hypothesize that mixing between iron-rich coastal waters and iron-limited Alaskan Gyre waters stimulated this bloom and fueled the high NCP and CO_2 export observed in the region.

Citation: Palevsky, H. I., F. Ribalet, J. E. Swalwell, C. E. Cosca, E. D. Cokelet, R. A. Feely, E. V. Armbrust, and P. D. Quay (2013), The influence of net community production and phytoplankton community structure on CO_2 uptake in the Gulf of Alaska, *Global Biogeochem. Cycles*, *27*, doi:10.1002/gbc.20058.

1. Introduction

[2] The ocean is a major sink for atmospheric carbon dioxide. Current estimates indicate that the ocean absorbs an estimated 2.0 ± 1.0 Pg C yr^{-1} [*Takahashi et al.*, 2009], which comprises ~25% of current annual carbon emissions from fossil fuel burning [*Le Quéré et al.*, 2009; *Friedlingstein et al.*, 2010]. The ocean's capacity to take up atmospheric CO_2 is driven by ocean circulation as well as two "carbon pumps"—the biological pump, by which CO_2 is taken up by photosynthetic organisms and exported to the deep ocean, and the temperature-driven solubility pump [*Volk and Hoffert*, 1985]. Understanding the mechanisms driving these natural carbon sinks is important for predicting how these sinks will respond to—and in turn potentially influence—the future trajectory of climate change.

[3] The seasonal and spatial variability of oceanic carbon uptake and the relative importance of the solubility and biological carbon pumps throughout the ocean have received much attention in recent years [e.g., *Marinov et al.*, 2008; *Takahashi et al.*, 2002, 2009]. These global-scale analyses, however, occur at coarse spatial resolution dictated by the availability of discrete measurements, satellite coverage and model resolution, which may underrepresent the significance of small-scale regions of intense carbon export. Fine spatial-scale measurements have uncovered the presence of biological "hotspots" occurring in narrow regions of convergence between water masses with different limiting nutrients [e.g., *Ribalet et al.*, 2010]. Mixing between these water masses within a transition zone can fuel enhanced phytoplankton growth and a strengthened biological carbon pump, which could lead narrow transition zones of enhanced biological production to disproportionately influence regional carbon cycling. Relatively little is known about the significance of these transition zones to the overall oceanic carbon sink or about the role that phytoplankton community composition in these regions plays in driving high biological production and carbon export.

[4] Recent advancements in the ability to make high-spatial-resolution oceanographic measurements using continuous flow methods have enabled researchers to investigate the role of small-scale features in the global carbon cycle. The amount of organic carbon exported from the surface to

Additional supporting information may be found in the online version of this article.

[1]School of Oceanography, University of Washington, Seattle, Washington, USA.
[2]Pacific Marine Environmental Laboratory, NOAA, Seattle, Washington, USA.

Corresponding author: H. I. Palevsky, School of Oceanography, University of Washington, Box 355351, Seattle, WA 98195, USA. (palevsky@u.washington.edu)

0886-6236/13/10.1002/gbc.20058

the deep ocean represents the strength of the biological carbon pump. This carbon export can be quantified by estimating the rate of net community production (NCP), defined as gross photosynthetic production minus community respiration, from measurements of biological oxygen supersaturation [*Craig and Hayward*, 1987; *Emerson et al*., 1991]. Since argon has similar solubility to oxygen but is biologically inert, measuring the O_2/Ar gas ratio rather than O_2 concentration isolates biological effects on oxygen supersaturation by controlling for physical processes such as bubble injection and temperature changes that can affect gas saturation [*Emerson et al*., 1991]. Continuous underway measurements of the dissolved O_2/Ar gas ratio using equilibrator inlet mass spectrometry (EIMS) combined with a wind-speed-based parameterization of air-sea gas exchange make it possible to estimate NCP at kilometer-scale resolution [*Tortell*, 2005; *Cassar et al*., 2009; *Stanley et al*., 2010] . Recently, it has become possible to characterize the phytoplankton community composition and abundance at similar kilometer-scale resolution using underway flow cytometry [*Cunningham et al*., 2003; *Thyssen et al*., 2009; *Swalwell et al*., 2011].

[5] We combined underway flow cytometry and dissolved gas measurements to evaluate phytoplankton community structure, NCP and CO_2 uptake across the transition zone from the Alaskan Gyre to coastal waters off the Aleutian Islands during a cruise across the Gulf of Alaska in May 2010 (Figure 1a). The Alaskan Gyre is an iron-limited high-nitrate low-chlorophyll (HNLC) ocean region [*Martin and Fitzwater*, 1988] while the coastal waters are iron-replete and seasonally nitrate-limited [*Whitney et al*., 2005], creating the potential for enhanced production where the Alaskan Gyre and coastal water masses converge. We discuss the significance of the transition zone to overall biological export and carbon uptake in the Gulf of Alaska during the time of our study, potential explanations for the observed strong biological carbon export in the transition zone and the significance of a distinct phytoplankton community found in this region.

2. Methods

[6] All samples were collected under way from the continuous seawater flow-through system of the R/V Thomas G. Thompson (5 m depth) on a transit from Seattle, WA to Dutch Harbor, AK from 3–8 May 2010 (Figure 1a).

2.1. Underway Measurements of Temperature, Salinity, Chlorophyll-a and Nitrate

[7] Sea surface temperature (SST) and salinity were measured using a shipboard Sea-Bird Electronics SBE-21 thermosalinograph. Chlorophyll-a fluorescence was measured using a shipboard WET Labs ECO FLRTD chlorophyll fluorometer. Nitrate concentrations were measured using a Satlantic ISUS nitrate sensor. Discrete samples for salinity, chlorophyll-a and nitrate collected shortly after the completion of the cruise during subsequent work in the Bering Sea were used to create calibration curves to correct the underway measurements. Underway salinity measurements were calibrated using discrete samples collected 11 May–25 June 2010 (n = 58) and analyzed using standard methods on a Guildline Autosal laboratory salinometer, with calibrated values accurate to ±0.23. Underway fluorescence-based estimates of chlorophyll-a were calibrated using discrete samples collected 11 May–2 June 2010 (n = 28) and analyzed following the acidification method [*Lorenzen*, 1966] on a Turner Designs 10-AU fluorometer, with calibrated values for the underway measurements accurate to ±0.70 μg/L. Underway nitrate concentrations were detrended to account for drift due to aging of the sensor's ultraviolet light source and calibrated using samples collected 11 May–13 July 2010 (n = 94) and analyzed following methods modified from *Armstrong et al*. [1967]. Calibrated values for the underway nitrate measurements are accurate to ±1.2 μM.

2.2. Underway Measurements of O_2/Ar and Estimating NCP

[8] High spatial resolution (~4 km) underway measurements of O_2/Ar along the cruise track were made using continuous flow equilibrator inlet mass spectrometry (EIMS) following procedures similar to those described by *Cassar et al*. [2009]. EIMS-based measurements were calibrated by correcting for instrumental drift with regularly sampled ambient air and correcting for instrumental offset based on isotope ratio mass spectrometer O_2/Ar measurements on discrete samples (n = 4) following the collection procedures of *Emerson et al*. [1995] and the analytical procedures of *Juranek and Quay* [2005]. From a measured O_2/Ar ratio, the biological oxygen supersaturation can be defined as:

$$\Delta O_2/Ar = \left[(O_2/Ar)_{sample}/(O_2/Ar)_{sat}\right] - 1 \quad (1)$$

where $(O_2/Ar)_{sample}$ is the measured O_2/Ar ratio and $(O_2/Ar)_{sat}$ is calculated based on the temperature- and salinity-dependent solubility of both gases [*Garcia and Gordon*, 1992; *Hamme and Emerson*, 2004]. Propagation of 0.2% error in air standards run along with the discrete samples and error in the discrete sample correction factor applied to EIMS data yield a precision in calculated ΔO_2/Ar of ±0.3%.

[9] In conditions approaching steady state with negligible vertical entrainment, diffusion, and advection, ΔO_2/Ar in the surface mixed layer reflects a balance between net biological production (consumption) of oxygen and net air-sea O_2 gas evasion (invasion). NCP can thus be calculated based on a simplified gas budget approach:

$$NCP = k_{O2} * [O_2]_{sat} * (\Delta O_2/Ar) * \rho \quad (2)$$

where k_{O2} (m d^{-1}) is the air-sea gas transfer velocity, $[O_2]_{sat}$ (μmol kg^{-1}) is the temperature- and salinity-dependent O_2 concentration at saturation [*Garcia and Gordon*, 1992], and ρ (kg m^{-3}) is the seawater density. k_{O2} was calculated along the cruise track using satellite-derived wind speed data (see section 2.6) and a time-weighted parameterization of gas exchange [*Reuer et al*., 2007] based on the *Nightingale et al*. [2000] dependence of k_{O2} on wind speed and the temperature- and salinity-dependent Schmidt number [*Wise and Houghton*, 1966; *Wanninkhof*, 1992]. Recent wind-speed-based parameterizations of gas exchange have converged to produce values of k similar to that of Nightingale et al. [e.g., *Ho et al*., 2006; *Sweeney et al*., 2007], so we quantified uncertainty in k_{O2} by assuming that the spread in the wind-speed-based parameterizations generated by *Wanninkhof* [1992] and *Liss and Merlivat* [1986], which fall well above and below the convergence of more recent values, bracket 95% of the k_{O2}

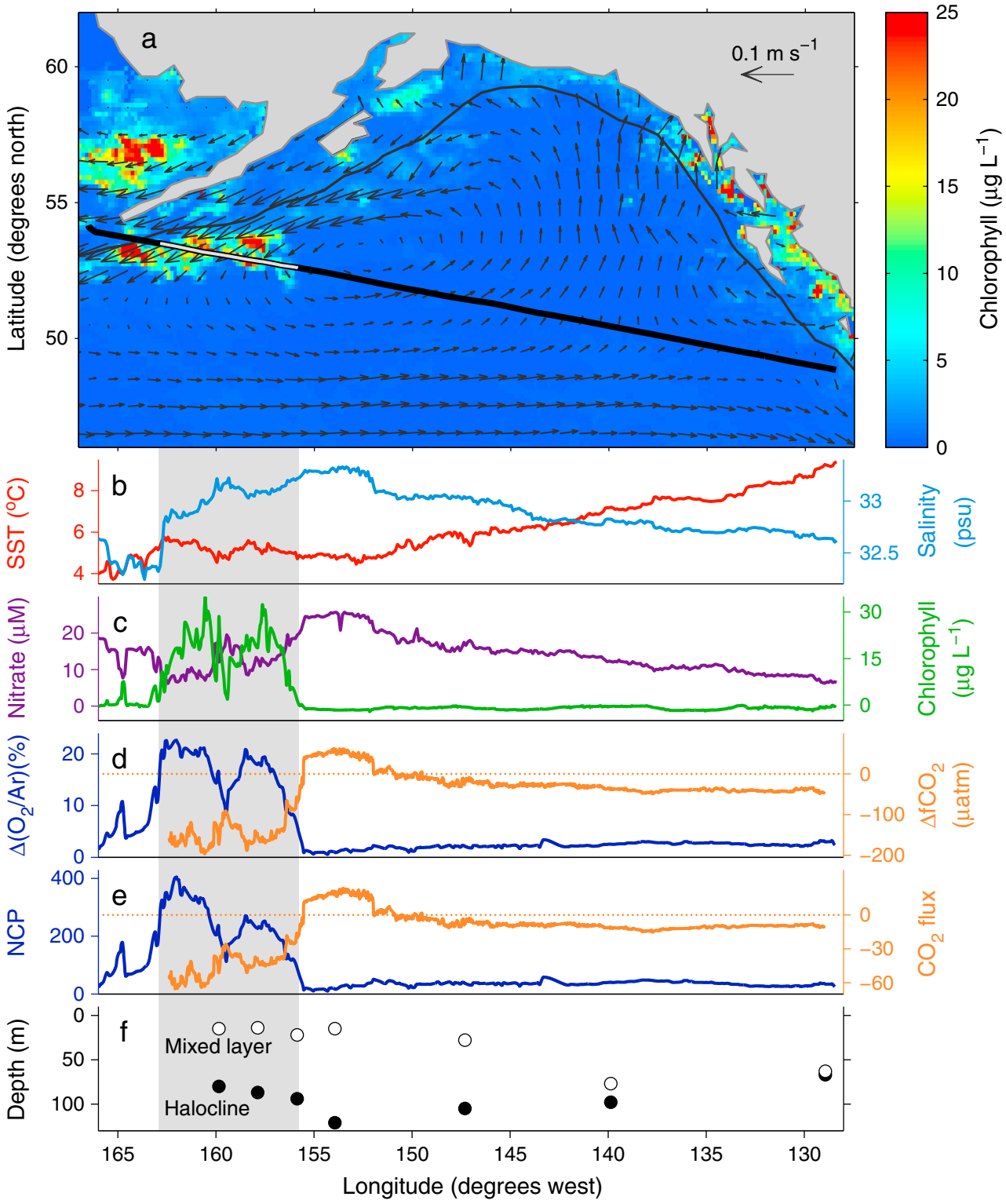

Figure 1. (a) Satellite-based surface currents and chlorophyll-a concentrations (µg/L) in the Gulf of Alaska at the time of this study. The 2000 m isobath indicates the location of the continental slope. The cruise track is in black, with the transition zone highlighted in gray. The transition zone is differentiated from the Alaskan Gyre to the east and coastal region to the west based on elevated surface chlorophyll-a concentrations. (b) Sea surface temperature (SST) and salinity, (c) surface nitrate and chlorophyll-a concentrations, (d) $\Delta O_2/Ar$ and ΔfCO_2, (e) NCP and air-sea CO_2 flux (negative values indicate oceanic uptake of CO_2) along the cruise track, calculated from $\Delta O_2/Ar$ and ΔfCO_2 following equations (2) and (3), respectively, both in units of mmol C m^{-2} d^{-1}. (f) Estimated mixed layer depth (MLD) and halocline depth from seven Argo depth profiles along the cruise track. The transition zone is highlighted in gray in all plots.

variability (±2σ). Combining this spread of parameterizations with error introduced into the time-weighting by uncertainty in MLD calculations (see section 2.5), we estimate that our parameterization of k_{O2} is accurate to ±15–20% (1σ), with variation in uncertainty across the cruise track due to wind speed variations. The uncertainty in NCP values ranges from 15–55% with a median uncertainty of 20% that reflects the combination of this location-specific uncertainty due to gas exchange parameterization and uncertainty in $\Delta O_2/Ar$. Regional mean data are presented with error representing a 1σ confidence interval in the NCP estimate rather than spatial variability across the region. To calculate NCP in carbon rather than oxygen units, we converted using a ratio of 1 C: 1.4 O_2 [*Laws*, 1991].

2.3. Underway Measurements of fCO_2 and Estimating Air-Sea CO_2 Flux

[10] An underway IR-detection-based system (previously described in detail by *Feely et al*., [1998] and *Pierrot et al*., [2009]) was used to make continuous measurements of surface ocean and atmospheric fugacity of CO_2 (fCO_2) accurate to ±2 μatm. Due to a shorter integration time in the CO_2 equilibrator system than in the EIMS O_2/Ar measurements, fCO_2 is measured at a spatial resolution finer than that of EIMS-based measurements (~1 km versus ~4 km for EIMS). The net air-sea flux of CO_2 is calculated based on the air-sea gradient in fCO_2 (ΔfCO_2):

$$\text{Air-sea } CO_2 \text{ flux} = k_{CO2} * K_0 * \Delta fCO_2 * \rho \quad (3)$$

where k_{CO2} (m d^{-1}) is the air-sea gas transfer velocity, calculated as described above, K_0 (mol kg^{-1} atm^{-1}) is the temperature- and salinity-dependent solubility of CO_2 [*Weiss*, 1974], ΔfCO_2 (μatm) = $fCO_{2,ocean} - fCO_{2,atmosphere}$, and ρ (kg m^{-3}) is the seawater density. Where the air-sea CO_2 flux is negative, the ocean takes up CO_2 from the atmosphere. The uncertainty in air-sea CO_2 flux values ranges from 15–100% with a median uncertainty of 29% that reflects both uncertainty in k_{CO2} (±15–20%, as explained above) and uncertainty in ΔfCO_2 measurement, with regional mean data presented with error representing a 1σ confidence interval in the CO_2 flux estimate rather than spatial variability across the region.

2.4. Underway Flow Cytometry Measurements

[11] Continuous underway measurements of phytoplankton abundance and composition were made using SeaFlow, a flow-through cytometer that utilizes light scattering and cellular autofluorescence properties of individual cells to discriminate phytoplankton populations that span 1–20 μm in nominal cell size [*Swalwell et al*., 2011]. Data files were created every 3 min, yielding a sampling resolution along the cruise track of ~1 km. Data were analyzed using the R package *flowPhyto* [*Ribalet et al*., 2011], which uses statistical clustering methods to automate the identification of phytoplankton populations. Populations were distinguished based on five analysis parameters: forward scatter (a proxy for cell size) in orthogonal and perpendicular polarization states, red fluorescence from chlorophyll (collected using a 692-40 band-pass filter), a second red fluorescence chlorophyll detector for large particles, and orange fluorescence from phycoerythrin (collected using a 527-27 band-pass filter). A change point detection algorithm developed by *Aghaeepour et al*. [2011] was used to determine the optimal number of populations present in each sample. When necessary, files were concatenated so a sufficient number of cells (at least 300) were present in order to perform aggregate statistics for each population. To generate an estimate of the phytoplankton biomass observed by SeaFlow, a total chlorophyll proxy that sums the size-weighted contributions of all phytoplankton populations was calculated using population-specific cell concentrations, estimates of population-specific cell size based on light scattering, size-specific cell volume to cell carbon ratios (mean of values from *Booth et al*. [1988], *Verity et al*. [1992], and *Montagnes et al*. [1994]), and a carbon:chlorophyll ratio of 60:1 [*Frost*, 1993]. We estimate that this total chlorophyll proxy is accurate to ±60%, assuming an uncertainty of ±30% in cell size estimates, ±40% in cell volume to cell carbon ratios (reflecting the standard deviation of the three literature values for each population), and ±30% in the carbon:chlorophyll ratio.

2.5. Halocline and Mixed Layer Depths (MLDs)

[12] Mixed layer and halocline depths along the cruise track were estimated based on depth profiles of temperature and salinity measured on seven Argo floats during the same time period as shipboard sampling (3–8 May 2010), with surface-most measurements at 4 m and depth resolution of 10 m from 10 to 300 m. Argo profiles were taken from within 12.5 km of the cruise track with the exception of a single profile representative of the open Alaskan Gyre region (147.3°W) taken 75 km from the cruise track.

[13] MLD was calculated based on density change from the reference depth of 4 m. Due to thermal stratification induced by springtime surface warming, MLD at some locations was sensitive to the selection of a density change criterion ($\Delta\sigma_\theta$). A range of criteria have commonly been applied both worldwide and in the North Pacific, from 0.03 kg m^{-3} [*De Boyer Montégut et al*., 2004; *Thomson and Fine*, 2003] to 0.125 kg m^{-3} [*Monterey and Levitus*, 1997; *Suga et al*., 2004]. The intermediate criterion of $\Delta\sigma_\theta = 0.08$ kg m^{-3} was selected to most accurately reflect MLDs estimated by visual inspection of the individual depth profiles to account for the effects of thermal stratification. The full range of criteria from 0.03 kg m^{-3} to 0.125 kg m^{-3} was used to calculate ranges of potential MLDs over the period of stratification, which were used to calculate uncertainty in the time-weighted parameterization of k_{O2}. Halocline depth was calculated using salinity change criteria (ΔS) from 4 m of 0.25.

2.6. Satellite-Based Data

[14] The following satellite-based data were used in this study: 5-day averaged surface current velocity and direction from OSCAR (http://www.oscar.noaa.gov); dynamic sea surface height anomalies from AVISO (http://www.aviso.oceanobs.com); MODIS 8-day averaged sea surface temperatures and chlorophyll-a concentrations and net primary production rates calculated using the vertically generalized production model (VGPM) [*Behrenfeld and Falkowski*, 1997] and the carbon-based production model (CbPM) [*Westberry et al*., 2008] from the Oregon State Ocean Productivity site (http://www.science.oregonstate.edu/ocean.productivity); and daily wind speeds from the NOAA National Climatic Data Center (NCDC)'s multiple-satellite Blended Sea Winds product (http://www.ncdc.noaa.gov/oa/

rsad/air-sea/seawinds.html). The NOAA NCDC Blended Sea Winds (0.25° gridded global resolution) were validated for our study by comparison of daily satellite-based wind speeds at Ocean Station Papa (OSP, 50°N, 145°W) from the time of the cruise and sixty days prior with mooring-based daily-averaged wind speed measurements at OSP (http://www.pmel.noaa.gov/stnP) from the same time period, corrected to 10 m above sea level, resulting in a root mean squared error of 1 m s^{-1} with no systematic bias. This accuracy is comparable to that found in a previous comparison between NOAA NCDC Blended Sea Winds and a global data set of buoy wind observations [*Bentamy et al.*, 2009].

3. Results and Discussion

3.1. Regional Setting

[15] Circulation in the Gulf of Alaska is dominated by the cyclonic Alaskan Gyre with geostrophically driven surface currents, as can be seen from satellite-derived surface current data from the time of the cruise (Figure 1a). The shelf region is dominated by the Alaska Coastal Current (ACC), which is driven west along the coastline by alongshore winds and significant freshwater runoff [*Stabeno et al.*, 2004] and the Alaskan Stream, which flows southwest along the Alaskan Peninsula slope, offshore of the ACC, as the western boundary current of the Alaskan gyre [*Favorite et al.*, 1976; *Stabeno et al.*, 2004]. Our data show a strong salinity front over the continental slope (Figure 1b), with low salinity inshore of this front (west of 162.9°W) consistent with the expected low salinity signature of the Alaskan Stream (<32.6 psu, [*Favorite et al.*, 1976]).

[16] Satellite-based chlorophyll-a concentrations indicate that the highest phytoplankton biomass in the Gulf of Alaska at the time of our study occurred just east of this salinity front, offshore of the Alaskan Peninsula slope (Figure 1a). This high-chlorophyll feature was evident from measurements along the cruise track, which show a region of elevated chlorophyll-a concentrations reaching 30 µg L^{-1} that extended from 162.9°W to 155.8°W, between the continental slope salinity front to the west and the center of the Alaskan gyre circulation to the east (Figure 1c). This region of elevated chlorophyll along the cruise track was marked by surface waters that were warmer and fresher than the adjacent open Gulf of Alaska region, with decreased nitrate concentrations and elevated O_2/Ar supersaturation, fCO_2 undersaturation, NCP and CO_2 uptake, and shallow mixed layers (Figures 1b–1f). For the purposes of this paper, this region of elevated chlorophyll-a concentration is defined as a transition zone, with the Alaskan Gyre to the southeast and the coastal region to the northwest.

[17] Although this transition zone is primarily distinguished based on high phytoplankton biomass, the distinction among the three regions is also supported by different nitrate-salinity (NO_3-S) relationships (Figure 2). The Alaskan Gyre region shows a consistent linear relationship between nitrate concentrations and salinity ($r^2 = 0.90$, $p < 0.01$), similar to that previously described in depth profiles from straits through the Aleutian Islands [*Mordy et al.*, 2005] and the northern coastal Gulf of Alaska [*Childers et al.*, 2005; *Ladd et al.*, 2005]. Data from the P17N CLIVAR line across the Gulf of Alaska (Stations 71–77: 50°N, 152°W to 55.5°N, 152.9°W; data not shown) during the end of the winter season in March 2006

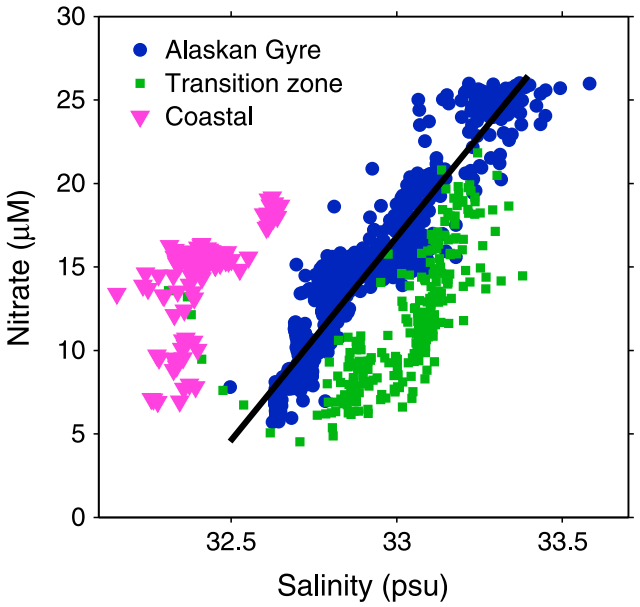

Figure 2. Sea surface nitrate concentrations plotted versus salinity for all regions along the cruise track. The linear regression for the Alaskan Gyre region ($r^2 = 0.90$, $p < 0.01$) is shown in black.

showed the same linear NO_3-S relationship in surface water and in depth profiles, indicating that this relationship extends to surface waters prior to spring biological nitrate drawdown. This suggests that the strong NO_3-S relationship observed in Alaskan Gyre surface waters in May 2010 reflects entrainment of deep nutrient-rich, higher salinity water during the winter as the mixed layer deepens down to the permanent halocline (Figure 1f), with little subsequent nitrate drawdown by the time of the cruise. Water masses from the coastal region and transition zone do not fall on this line. The coastal water is distinctly fresher than the Alaskan Gyre waters but with higher nitrate concentrations than would be predicted by the Alaskan Gyre NO_3-S relationship, reflecting significant freshwater input from the Alaskan Stream and ACC. The transition zone is distinguished by nitrate concentrations that are consistently lower than the observed linear NO_3-S relationship from the Alaskan Gyre for a similar range in salinity, reflecting either biological nitrate drawdown or a contribution from a water mass with a different NO_3-S relationship than the Alaskan Gyre.

3.2. Estimates of NCP and CO_2 Flux from ΔO_2/Ar and ΔfCO_2

[18] The trends in dissolved gas concentrations (ΔO_2/Ar and ΔfCO_2) rather than variations in gas transfer velocities were the dominant terms when calculating NCP and CO_2 flux rates from equations (2) and (3), although variations in wind speed across the cruise track yielded gas transfer velocities (k_{O2} and k_{CO2}) ranging from 4.5 to 9.8 m d^{-1} (Figures 1d and 1e). Gas residence times (i.e., mixed layer depth / gas transfer velocity) in the Alaskan Gyre ranged from 2–14 days while the shallower mixed layer depths in the transition zone and coastal region (Figure 1f) led to shorter gas residence times of 2–4 days. While the Alaskan Gyre region more closely approximates steady state conditions than the transition zone and coastal regions, these short residence times

Table 1. Summary of NCP Rates From Open Ocean and Coastal Studies in the Gulf of Alaska

	May	Annual	
	(mmol C m^{-2} d^{-1})	(mol C m^{-2} yr^{-1})	Source
Alaskan Gyre	17[a]	2.5	*Emerson and Stump* [2010]
	9–12[a]	(1.6)[b]	*Emerson et al.* [1991]
	15[a]	(2.1 ± 1.5)[b]	*Emerson* [1987]
	7.1		*Charette et al.* [1999]
	26.6[a]		*Wheeler* [1993] (NO_3 budget)
	21.3 ± 2.2[a]		*Wheeler* [1993] (^{15}N incubations)
	(20.3)[a,b]	3.05	*Wong et al.* [2002]
	35.1 ± 8.9		This study
Transition zone and coastal region		3.89	*Wong et al.* [2002]
	249 ± 40 (transition)		This study
	88.0 ± 14.5 (coastal)		

[a]Whole-summer rather than May values.

[b]Parentheses denote values calculated based on *Emerson and Stump*'s [2010] conclusion (based on year-round data from a mooring at OSP) that summer production occurring over 150 days drives essentially all annual biological carbon export, with little or no net export production in winter.

support the applicability of the steady state model used to calculate NCP and CO_2 flux in the transition zone and coastal regions despite the fast current speeds (i.e., at the maximum observed current velocity, water would only be advected ~30 km during the maximal 4 day gas residence time).

[19] During the time of the cruise, $\Delta O_2/Ar$ in the Alaskan Gyre was consistently supersaturated (2.2% ± 0.3%), indicating net autotrophic conditions with a mean NCP rate of 35.1 ± 8.9 mmol C m^{-2} d^{-1}. This is slightly higher than previously measured values in this region, where summer NCP estimates based on gas and nitrate budgets have ranged from 9 to 27 mmol C m^{-2} d^{-1} (Table 1). Surface ocean fCO_2 was undersaturated in the portion of the Alaskan Gyre east of the gyre center, while at the gyre center (152.2°W to 155.5°W), surface ocean fCO_2 was supersaturated with respect to the atmosphere, indicating net CO_2 outgassing (mean air-sea CO_2 flux of 15.7 ± 3.2 mmol C m^{-2} d^{-1}) consistent with an input of entrained deep water from winter mixing as suggested by the NO_3-S relationship (Figure 2). Overall, the Alaskan Gyre region was a net CO_2 sink (mean air-sea CO_2 flux of −5.1 ± 1.2 mmol C m^{-2} d^{-1}), with a slightly higher rate of CO_2 uptake than previously reported at OSP in the month of May [*Wong and Chan* 1991] (Table 2). This region is also a net CO_2 sink on an annual basis, with estimates of air-sea CO_2 flux in the Alaskan Gyre ranging from −1.7 to 0 mol C m^{-2} yr^{-1} (Table 2). Ecosystem/carbon flux model simulations comparing a biotic to an abiotic ocean at OSP indicate that biological production plays an important role in driving net carbon uptake in this region [*Signorini et al.*, 2001].

[20] The maximum $\Delta O_2/Ar$ supersaturation (up to 22.7%) and fCO_2 undersaturation (fCO_2 down to 196 μatm) along the cruise track were observed in the transition zone. NCP and CO_2 uptake rates varied in concert, with a high degree of correlation ($r^2 = 0.73$, $p < 0.01$) throughout the transition zone, indicating that the CO_2 uptake in this region was primarily driven by biological production. NCP rates were ~6× higher than CO_2 uptake rates, which is the result of the mixed layer O_2 budget being dominated by NCP and O_2 gas exchange with a short air-sea equilibration time (days) whereas the mixed layer CO_2 budget is dominated by NCP and physical CO_2 supply with a longer air-sea equilibration time (months). Coincident with high chlorophyll-a concentrations, two distinct peaks of elevated NCP and CO_2 uptake were observed in the transition zone, yielding a mean transition zone NCP rate of 249 ± 40 mmol C m^{-2} d^{-1} and mean transition zone air-sea CO_2 flux of −42.3 ± 6.1 mmol C m^{-2} d^{-1}. These NCP and CO_2 uptake rates are large as compared to those previously reported for the Gulf of Alaska (Tables 1 and 2). Although little attention has previously been focused on this transition zone region, strong negative ΔpCO_2 values for the region off the Aleutian Peninsula were measured in summer (May–August) during repeated surface pCO_2 transects across the North Pacific, including surface water pCO_2 as low as 150 μatm measured in May 1997 [*Murphy et al.*, 2001; *Zeng et al.*, 2002]. Such high NCP and CO_2 uptake rates have been previously observed elsewhere in ocean margin regions experiencing episodic periods of high biological production. During the eastern Bering Sea spring bloom, NCP can reach rates of 360–1300 mmol C m^{-2} d^{-1} [*Prokopenko et al.*, 2010], while eastern north Pacific coastal upwelling systems can produce NCP rates of up to 1200 ± 420 mmol C m^{-2} d^{-1}on the

Table 2. Summary of Air-Sea CO_2 Flux Rates From Open Ocean and Coastal Studies in the Gulf of Alaska

	May	Annual	
	(mmol C m^{-2} d^{-1})	(mol C m^{-2} yr^{-1})	Source
Alaskan Gyre	−3.5, −4.4	−0.7	*Wong and Chan* [1991]
		−0.6	*Chierici et al.* [2006]
		−1.7–0	*Takahashi et al.* [2009]
	−5.1 ± 1.2		This study
Transition zone and coastal region	−27.6 ± 6.7[a]		*Ribalet et al.* [2010]
		−1.8	*Chen and Borges* [2009]
	−42.3 ± 6.1		This study

[a]June rather than May values.

continental shelf [*Fassbender et al*., 2011] and summer air-sea CO_2 flux rates of −20 mmol C m^{-2} d^{-1} [*Hales et al*., 2005].

[21] Mean NCP rates (88.0 ± 14.5 mmol C m^{-2} d^{-1}) in the coastal region were higher than in the Alaskan Gyre and higher than previous coastal measurements (Table 1), but were considerably lower than in the transition zone. fCO_2 measurements and estimates of CO_2 uptake did not extend into the coastal region.

3.3. Phytoplankton Abundance and Community Composition

[22] Clustering analysis of the flow cytometry measurements revealed six phytoplankton populations present along the cruise track. Five populations were distinguished based on red fluorescence from chlorophyll-a and forward angle light scatter (a proxy for size): ultraplankton, larger and smaller nanoplankton, and larger and smaller elongated phytoplankton (Figure S1a in the supporting information). Elongated cells were identified by low light scattering relative to their red fluorescence, due to the long and narrow cell shape [*Olson et al*., 1989]. *Olson et al*. [1989] identified elongated cells with a similar cytometric signature as pennate diatoms, though the identity of the elongated populations in this study cannot be verified, as cells were not collected for microscopic analysis. A sixth population, the cyanobacteria *Synechococcus*, was identified by the unique orange fluorescence signal characteristic of its phycoerythrin pigment (Figure S2b in the supporting information).

[23] There is a strong correlation ($r^2 = 0.89$, $p < 0.001$) between the cytometry-based total chlorophyll proxy summing the size-weighted contributions of each of these six phytoplankton populations to total chlorophyll and chlorophyll-a concentrations independently calculated from bulk fluorescence (Figure 3a). Despite significant uncertainty (60%) in the cytometry-based total chlorophyll proxy, this result suggests that phytoplankton >20 μm did not provide a major contribution to the overall phytoplankton biomass (as cells >20 μm would have been outside the flow cytometer size detection limit). The percent contribution of each of the six phytoplankton populations to the cytometry-based total chlorophyll proxy was calculated for each region, with uncertainty introduced in estimating cell size, carbon content, and the carbon:chlorophyll ratio from literature values (Table 3).

[24] Chlorophyll-a concentrations were low across the Alaskan Gyre (mean of 0.27 μg L^{-1} from MODIS observations; indistinguishable from zero based on the shipboard fluorometer). This is consistent with expected low phytoplankton production rates in the iron-limited HNLC gyre and with long-term monthly chlorophyll-a measurements at OSP that are consistently <0.4 μg/L throughout the annual cycle [*Harrison et al*., 1999]. The phytoplankton community (Figure 3) was mainly composed of *Synechococcus* and ultraplankton with a lesser contribution from smaller elongated phytoplankton, which is consistent with previous observations at OSP of phytoplankton populations dominated by *Synechococcus* and other phytoplankton <5 μm with sparse small pennate diatoms [*Booth et al*., 1993; *Boyd and Harrison*, 1999]. Although numerically abundant, *Synechococcus* cells contributed to only 5 ± 9% of the total chlorophyll proxy in the Alaskan Gyre region due to their relatively small size, while smaller elongated phytoplankton and ultraplankton contributed to 37 ± 19% and 30 ± 18%, respectively, of the total chlorophyll proxy.

[25] The phytoplankton community composition changed dramatically at the transition zone, corresponding with the increase in chlorophyll-a concentrations (Figure 3). Mean chlorophyll-a concentrations (17.1 μg/L) in the transition zone are high compared to previous observations in the region, although chlorophyll-a concentrations >13 μg/L have been measured at inshore locations in the northern Gulf of Alaska [*Childers et al*., 2005; *Strom et al*., 2006]. While measured fluorescence-based chlorophyll-a in this region may have been enhanced due to photoacclimation of cells during deep mixing prior to this bloom or species-specific variation in the relationship between cellular fluorescence and chlorophyll-a [*Sosik et al*., 1989], such high chlorophyll-a concentrations clearly represent a large bloom. The transition zone comprises only 25% of the total area where flow cytometry measurements were made in crossing the Gulf of Alaska but contributed 66% of the total phytoplankton biomass (as estimated from the cytometry-based total chlorophyll proxy) observed along the cruise track, highlighting the importance of the phytoplankton community in this region.

[26] The transition zone was marked by two distinct phytoplankton communities corresponding with the peaks in chlorophyll-a, NCP and CO_2 uptake. The eastern side of the transition zone was dominated by the larger and smaller nanoplankton populations with a lesser contribution from smaller elongated phytoplankton, while the western side was dominated by larger nanoplankton with significant contributions from both larger and smaller elongated phytoplankton, ultraplankton, and *Synechococcus*, reflecting a shift in the phytoplankton community across the transition zone. The two nanoplankton populations together dominated contributions to the total chlorophyll proxy in the transition zone (73 ± 18%) but make up a much smaller proportion of the total across the rest of the cruise track (22 ± 17% in the Alaskan Gyre and 29 ± 18% in the coastal region). Across the entire cruise track, the larger and smaller nanoplankton and larger elongated phytoplankton populations (Figures 3b, 3d, and 3e) were predominantly found in the transition zone, suggesting that these populations were particularly adapted to transition zone conditions and were associated with high NCP and CO_2 uptake. The smaller nanoplankton population (Figure 3e) was found predominantly in the eastern side of the transition zone, highlighting the distinction between the phytoplankton communities in the eastern and western sides of this region. Both transition zone phytoplankton communities were distinct from the Alaskan Gyre phytoplankton community and the ultraplankton-dominated community in the coastal region. A similar feature with distinct phytoplankton populations uniquely found across a narrow spatial gradient was previously observed at the transition between the coastal and open HNLC regions of the Gulf of Alaska off the coast of British Columbia which was interpreted as reflecting changes in growth conditions as the two water masses converged and created distinct ecological niches promoting enhanced phytoplankton productivity [*Ribalet et al*., 2010].

[27] The small (<20 μm) phytoplankton populations that dominate the transition zone in this study were associated with high rates of NCP and CO_2 drawdown, which was unexpected given that larger, denser cells such as chain-forming

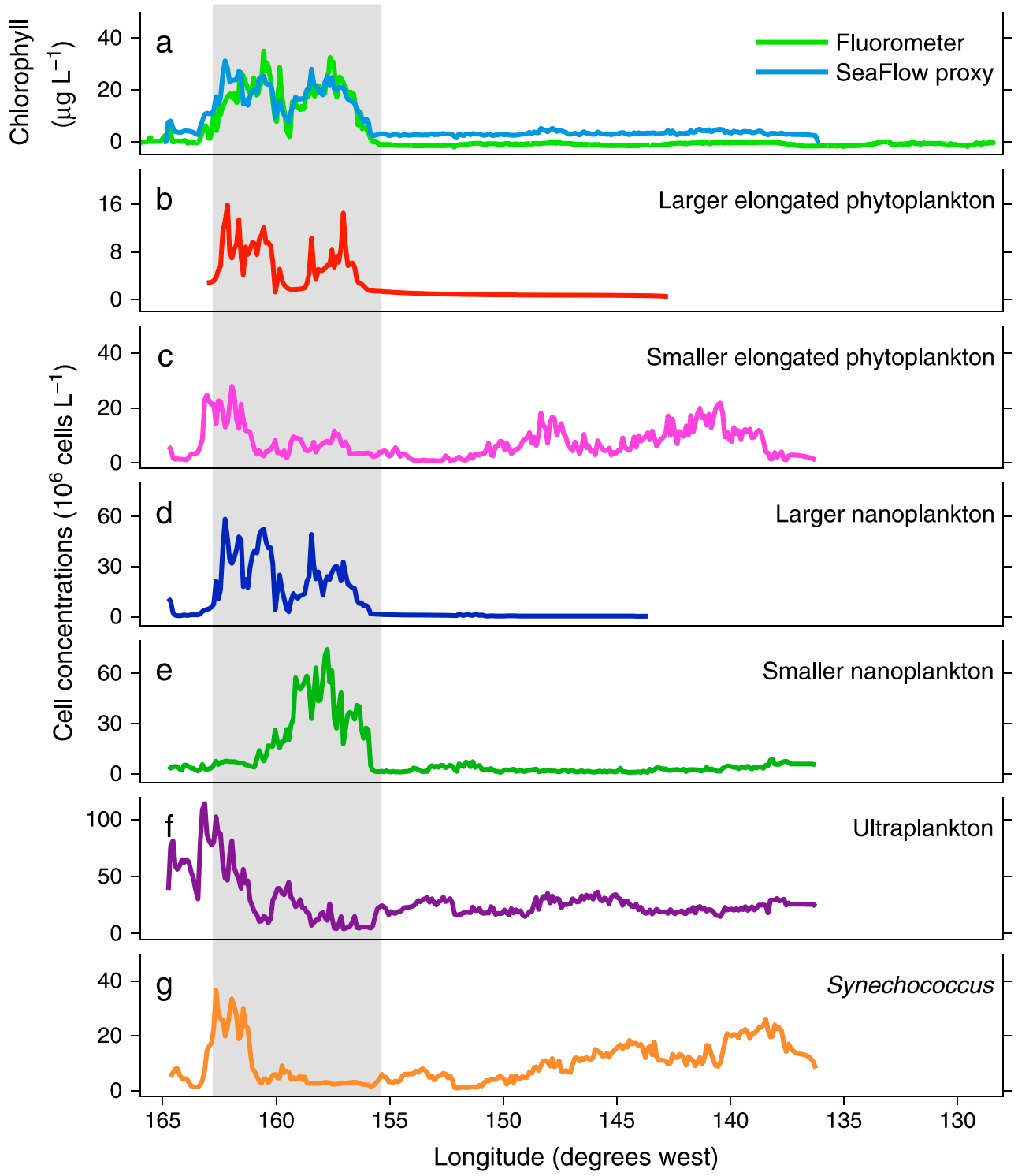

Figure 3. (a) Chlorophyll-a concentrations along the cruise track from fluorometry-based measurements and a cytometry-based proxy for total chlorophyll calculated based on estimates of cell-specific chlorophyll content for each phytoplankton population shown below. (b–g) Cell abundance along the cruise track for six phytoplankton populations identified by underway flow cytometry (see text and Figure S1 in the supporting information for description of clustering methods used to distinguish populations). Populations are ordered by nominal cell size from (Figure 3b) largest to (Figure 3g) smallest. The transition zone is highlighted in gray. The transition zone is differentiated from the Alaskan Gyre to the east and coastal region to the west based on elevated surface chlorophyll-a concentrations.

Table 3. Proportional Contribution of Phytoplankton Populations to Total Chlorophyll (proxy) by Region[a]

	Larger Elongated Phytoplankton	Smaller Elongated Phytoplankton	Larger Nanoplankton	Smaller Nanoplankton	Ultraplankton	*Synechococcus*	Mean Chlorophyll-a (μg/L)
Alaskan Gyre	6 ± 10%	37 ± 19%	6 ± 10%	16 ± 15%	30 ± 18%	5 ± 9%	0.27[b]
Transition zone	12 ± 14%	8 ± 12%	48 ± 20%	25 ± 17%	6 ± 10%	1 ± 4%	17.1
Coastal region	2 ± 7%	19 ± 16%	18 ± 16%	11 ± 13%	49 ± 20%	2 ± 7%	0.96

[a]Uncertainty in proportional contributions is calculated based on propagation of 60% uncertainty in the total chlorophyll proxy.
[b]Based on MODIS satellite observations, as chlorophyll-a estimates from the shipboard fluorometer were indistinguishable from zero.

diatoms are thought to lead to more efficient and higher rates of carbon export [*Smayda*, 1970; *Boyd and Newton*, 1995, 1999]. Previous studies have suggested that aggregation of cells and packaging by grazers can allow small cells to contribute more efficiently to carbon export [*Francois et al*., 2002; *Lutz et al*., 2007; *Richardson and Jackson*, 2007; *Kahl et al*., 2008; *Stukel et al*., 2011]. Further study will be necessary to evaluate the role of these mechanisms in the transition zone phytoplankton communities observed here.

3.4. Explaining Enhanced Biological Productivity in the Transition Zone

[28] A number of previous studies have suggested that increased iron availability at the convergence between iron-limited HNLC waters and iron-rich coastal waters in the Gulf of Alaska could stimulate phytoplankton production [e.g., *Whitney et al*., 2005; *Strom et al*., 2006; *Ribalet et al*., 2010]. Glacial meltwater input along the coast provides a source of particulate and dissolved iron to the ACC, which mixes with low-iron offshore waters to create a cross-shelf gradient in iron availability [*Wu et al*., 2009; *Lippiatt et al*., 2010]. Recirculation of flow from the Alaskan Stream into the Alaskan Gyre can transport iron-rich coastal waters offshore and stimulate phytoplankton production [*Favorite et al*., 1976; *Whitney et al*., 2005]. Mesoscale anticyclonic eddies, which propagate along the Alaskan Peninsula, can also supply coastally derived iron to offshore iron-limited waters [*Johnson et al*., 2005; *Lippiatt et al*., 2011; *Peterson et al*., 2011]. However, analysis of dynamic sea surface height anomalies (AVISO) does not provide evidence of eddies in the vicinity of the transition zone at the time of our cruise.

[29] Surface water properties along the cruise track show a distinct separation between the Alaskan Gyre and the coastal regions, with the coastal region particularly marked by a distinct freshwater signature (Figure 1b and Figure S2 in the supporting information). While there is a potential role for mixing between these water masses in the transition zone, this relationship is complex, as the Alaskan Stream supplies coastal water carried alongshore from the northeast, which may not match the properties of the coastal waters sampled along our cruise track. Mixing within the transition zone is heterogeneous, with two regions of pronounced warming and freshening corresponding with elevated chlorophyll-a concentrations (Figures 1b and 1c) and freshening correlated with increased NCP rates in the region east of the salinity front (Figure 4b; $r^2 = 0.62$, $p < 0.01$), suggesting that input of fresh coastal water contributed to elevated biological production.

[30] We therefore hypothesize that the high phytoplankton abundance and NCP rates in the transition region were fueled by coastal iron input to iron-limited Alaskan Gyre HNLC waters. Although iron concentrations were not measured during the cruise, this hypothesis is supported by previous measurements of total dissolved iron concentrations along the Alaskan Peninsula slope near the region of the transition zone, which were ~50-fold higher than at OSP, and corresponded with an increase in phytoplankton photosynthetic efficiency (F_v/F_m) as compared to the Alaskan Gyre [*Suzuki et al*., 2002]. It is also supported by the presence of the larger elongated phytoplankton population predominantly found in the transition zone (Figure 3b), which although only a minor contribution to the overall transition zone phytoplankton community (12 ± 14%), likely represents pennate diatoms such as *Pseudo-nitszchia* that have been shown to respond to addition of iron [*Marchetti et al*., 2006].

[31] It is noteworthy that while spring blooms do occur across the coastal region in the Gulf of Alaska, it is highly unusual for them to be as large as the transition zone bloom we observed. The coastal region of our study exhibited NCP rates and chlorophyll-a concentrations lower than those observed in the transition zone, though higher than those in the Alaskan Gyre. The coastal chlorophyll-a concentrations were within the range of previous observations of the May spring bloom period in the northern coastal Gulf of Alaska

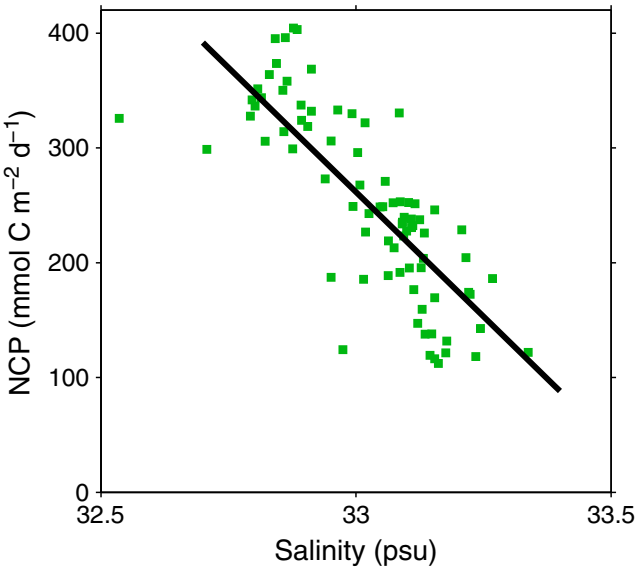

Figure 4. Transition zone NCP rates plotted versus salinity, with the linear regression ($r^2 = 0.62$, $p < 0.01$) shown in black.

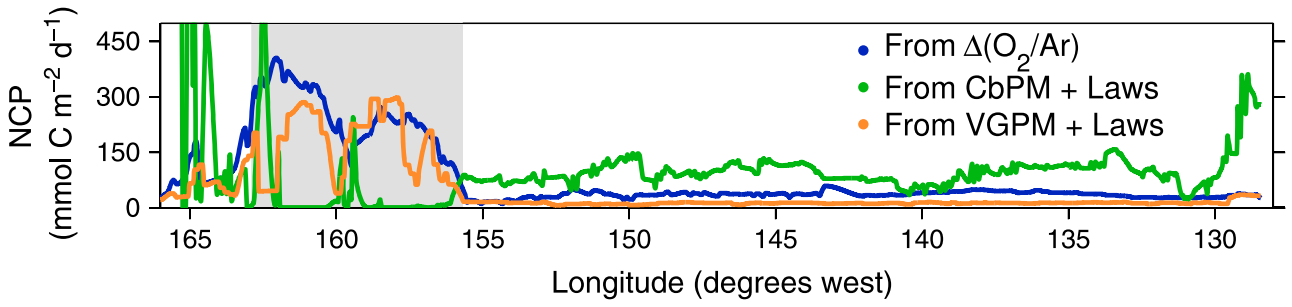

Figure 5. NCP rates calculated based on $\Delta O_2/Ar$ measured in this study plotted along with NCP rates calculated based on MODIS satellite data using the VGPM [*Behrenfeld and Falkowski*, 1997] and CbPM [*Westberry et al*., 2008] net primary production algorithms, each in combination with the export ratio algorithm of *Laws et al*. [2000]. The transition zone is highlighted in gray.

[*Strom et al*., 2006]. Onset of the spring phytoplankton bloom in the nutrient-replete inshore coastal Gulf of Alaska is triggered by relief of wintertime light limitation, with springtime cloud cover, extent of stratification and grazing pressure all influencing the timing and magnitude of these blooms [*Napp et al*., 1996; *Stabeno et al*., 2004]. Light availability could have limited phytoplankton production in the coastal region at the time of our study, although shoaling of mixed layers in response to spring thermal stratification observed from Argo floats in the transition zone may also have extended to the coastal region (where Argo floats were absent), which would have relieved light limitation and stimulated phytoplankton growth in both regions. Grazing pressure may also have reduced the size of the bloom in the coastal region if zooplankton growth kept pace with gradually increasing light availability and phytoplankton growth during spring. The transition zone, by contrast, was likely able to outstrip grazing pressure due to rapid phytoplankton response to addition of iron.

[32] The temporal evolution of the transition zone feature is an additional important consideration. Given the mean NCP rate of 249 mmol C m^{-2} d^{-1} calculated for the transition zone and assuming a starting nitrate concentration of the maximum observed along the cruise track (26 μM) and nitrate consumption at a rate of 106 C: 16 N [*Redfield et al*., 1963], biological drawdown would consume all the available nitrate in 12 days, suggesting that we sampled the transition zone in the midst of a short-lived bloom. Analysis of satellite-based surface chlorophyll data over the two-week intervals prior to and following our study indicate that highest chlorophyll concentrations and largest spatial extent of the bloom occurred during the 8-day interval spanning our 5-day cruise. This temporal evolution implies that the omission of a time rate of change term in the calculation of NCP and CO_2 flux rates in equations (2) and (3), which was based on the assumption of a steady state condition, potentially overestimated NCP rates. Without the inclusion of a time rate of change term, the biomass of organic carbon in the surface mixed layer that accumulated during the bloom (as indicated by satellite observations of increasing chlorophyll-a concentrations) was assumed to have been exported. However, it is possible that some of this carbon was later remineralized during the declining phase of this bloom rather than sinking out of the mixed layer and leading to export. Thus, the transition zone NCP estimates presented here are an upper limit on the amount of net carbon exported by the observed phytoplankton bloom. The observed shift in phytoplankton community structure across the transition zone may reflect the temporal evolution of the bloom as it spread across the transition zone region, with the two different phytoplankton communities in the eastern and western side of the region reflecting early and late stages of the bloom, as was suggested for the transition zone phytoplankton bloom described by *Ribalet et al*. [2010] in the northeast Pacific. Further study in this region will be necessary to determine the reasons for the distinct phytoplankton community compositions and the fate of organic carbon produced during short-lived transition zone bloom features.

3.5. Comparison with Satellite-Based Production Estimates

[33] This study presents a snapshot of conditions along our cruise track in the Gulf of Alaska in May 2010. Satellite observations provide a potentially powerful tool to extend this analysis to a broader spatial and temporal scale. Carbon export rates comparable to O_2/Ar-based estimates of NCP can be calculated from satellite-based estimates of net primary productivity (NPP), which is defined as gross photosynthetic production minus autotrophic respiration, multiplied by an estimate of the fraction of primary production exported from the surface ocean. Satellite-based models have previously applied this approach to calculate carbon export over the global ocean [*Muller-Karger et al*., 2005; *Dunne et al*., 2007], but there is relatively little observational data available to validate this approach.

[34] We compared our O_2/Ar-based NCP estimates with NCP rates calculated from satellite observations along the cruise track at the time of our study (integrated over 1–8 May 2010). We used publicly available NPP data calculated from the vertically generalized production model (VGPM) [*Behrenfeld and Falkowski*, 1997] or the carbon-based production model (CbPM), [*Westberry et al*., 2008]. The fraction of primary production exported from the surface ocean was calculated using the temperature- and NPP-based export ratio algorithm of *Laws et al*. [2000]. Satellite-based NCP rates calculated using the VGPM are correlated with O_2/Ar-based NCP rates from this study ($r = 0.67$, $p < 0.001$), while NCP rates calculated using the

CbPM do not correlate with O_2/Ar-based NCP rates and do not show the high-productivity features in the transition zone (Figure 5). The correlation between O_2/Ar- and VGPM-based NCP estimates is likely because the VGPM is a chlorophyll-based NPP model and ΔO_2/Ar-based NCP was strongly correlated with chlorophyll-a concentrations. The poor performance of the CbPM may reflect difficulty in using a backscattering-based NPP algorithm in a highly productive region.

[35] A number of factors may explain the differences between satellite-based and O_2/Ar-based NCP estimates across the cruise track. In the transition zone region, while the failure of the CbPM to identify the high-productivity features indicates a clear problem with application of the model to this region, the finding that VGPM-based NCP rates underestimate NCP as compared with O_2/Ar-based NCP estimates by ~1.5× may have been influenced by differences in temporal alignment of the two measurement techniques with peak bloom conditions, as O_2/Ar-based NCP estimates integrate over a 2–4 day gas residence time while the satellite-based NPP estimates integrate over an 8-day period. In the Alaskan Gyre region, however, which we expect was close to steady state conditions, temporal evolution should not affect the comparison between the estimates. Yet VGPM-based NCP estimates in the Alaskan Gyre region are ~3× lower than O_2/Ar-based NCP rates, while CbPM-based NCP estimates are ~2.5× higher than O_2/Ar-based rates, suggesting that there may be other important discrepancies among these two models and the *in situ* O_2/Ar-based estimates. These differences may reflect species- and condition-specific variations in carbon:chlorophyll ratios that may not be effectively captured by the chlorophyll-based VGPM, and variations in tendencies to aggregate, sink and export carbon that may not be fully captured in the *Laws et al*. [2000]. export ratio algorithm. The discrepancy between the satellite-based estimates of NCP and the O_2/Ar-based rates and the key finding that the CbPM failed to identify the transition zone bloom feature (Figure 5) highlight the need for more *in situ* NCP rate estimates to validate satellite-based rates on global, regional and local scales and particularly in high productivity hotspots such as the transition zone observed here.

4. Conclusions

[36] Observations of high NCP rates based on significant ΔO_2/Ar supersaturation and high CO_2 uptake rates in the transition zone between coastal waters along the Alaskan Peninsula and the HNLC Alaskan Gyre at the time of this study indicate that this was a region of strong biological production that drove significant uptake of atmospheric CO_2 during the observed bloom. In the transition zone, CO_2 uptake and NCP rates were 7–8× those in the Alaskan Gyre. The transition zone comprises only 20% of the total area covered in crossing the Gulf of Alaska but contributed 58% of the total NCP and 67% of the total CO_2 uptake observed along the cruise track. This narrow region thus played a key role in the overall carbon budget for the Gulf of Alaska during the time of our study.

[37] Correlation between the fluorescence-based bulk chlorophyll-a concentration, cytometry-based proxy of total chlorophyll, and NCP and CO_2 uptake rates suggest that CO_2 uptake in this region is likely dominated by small (<20 μm) abundant phytoplankton. The phytoplankton populations found predominantly in the transition zone form two different communities, each distinct from the communities in the Alaskan Gyre and coastal regions, suggesting that the transition zone forms a unique ecological niche for these populations. We hypothesize that mixing between iron-rich coastal waters and iron-limited Alaskan Gyre waters stimulated this bloom.

[38] The significant contribution of two nanoplankton populations distinguished by flow cytometry to the transition zone phytoplankton community suggests that these populations may be an important driver of the high NCP and CO_2 export observed in this region. Their dominance differentiates the transition zone bloom from coastal and iron-stimulated phytoplankton blooms previously observed in the Gulf of Alaska and North Pacific gyres, which are commonly dominated by large (>20 μm) chain-forming diatoms [*Boyd et al*., 1996, 2004; *Tsuda et al*., 2003; *Strom et al*., 2006]. Our observations of high NCP and CO_2 drawdown rates in the transition zone support the importance of small (<20 μm) phytoplankton cells to carbon export [*Richardson and Jackson*, 2007]. Further studies in this region should focus on identifying these phytoplankton populations and determining how they appear particularly well adapted to transition zone conditions and contribute so effectively to carbon export.

[39] The combination of continuous underway dissolved gas and flow cytometry methods enabled us to define narrow features not discernible with discrete measurements and to identify the potential importance of a distinct phytoplankton community to high regional uptake of atmospheric CO_2. NCP and CO_2 uptake rates of the magnitude observed in May in the transition zone exceed those reported previously in the Gulf of Alaska (Tables 1 and 2), with this narrow region providing the dominant contribution to total NCP and CO_2 uptake along the entire cruise track at the time of our study. Although satellite-based analysis potentially could be useful in determining the frequency and extent of such transition zone features, further calibration of satellite-based NCP estimates with observational data will be needed to quantify their contribution to total carbon export. The results presented here illustrate the importance of CO_2 uptake in a high productivity transition zone, and we hope they will motivate future investigation of the impact of these biological niches on carbon cycling, both in the Gulf of Alaska and in other ocean regions.

[40] **Acknowledgments.** We acknowledge and thank the following individuals and organizations: The captain and crew of R/V *Thomas G. Thompson*; Geoff Lebon and Dana Greeley who plumbed the ISUS nitrate sensor into the ship's underway seawater system; Jessica Cross and Nancy Kachel for collecting discrete water samples; Scott McKeever for analyzing discrete salinity samples; Calvin Mordy for supervising Eric Wisegarver who analyzed the discrete nitrate samples and Fred Menzia who analyzed the chlorophyll-a samples; Johnny Stutsman and Mark Haught for assistance in analyzing the discrete O_2/Ar samples; Steve Emerson and two anonymous reviewers for their valuable comments on the manuscript. Funding for this project was provided by a National Defense Science and Engineering Graduate fellowship from the Office of Naval Research and an ARCS Foundation fellowship to H.I.P., by NOAA OAR Climate Program Office grant A10OAR4310088 to P.D.Q. and E.V.A., by NSF grant 0622247 and a Gordon and Betty Moore Foundation Marine Microbiology Investigator award to E.V.A., by NOAA Ocean Climate Observation Program support for C.E.C. and R.A.F., and by the North Pacific Research Board's Bering Sea Program. This is contribution 3936 from NOAA's Pacific Marine Environmental Laboratory and contribution EcoFOCI-0794 from NOAA's Fisheries-Oceanography Coordinated Investigations.

References

Aghaeepour, N., R. Nikolic, H. H. Hoos, and R. R. Brinkman (2011), Rapid cell population identification in flow cytometry data, *Cytometry A*, *79*(1), 6–13, doi:10.1002/cyto.a.21007.

Armstrong, F. A. J., C. R. Stearns, and J. D. H. Strickland (1967), The measurement of upwelling and subsequent biological processes by means of the Technicon AutoAnalyzer and associated equipment, *Deep-Sea Res.*, *14*, 381–389.

Behrenfeld, M. J., and P. G. Falkowski (1997), Photosynthetic rates derived from satellite-based chlorophyll concentration, *Limnol. Oceanogr.*, *42*(1), 1–20.

Bentamy, A., C. Croize-Fillon, P. Queffeulou, C. Liu, and H. Roquet (2009), Evaluation of high-resolution surface wind products at global and regional scales, *J. Oper. Ocean.*, *2*(2), 15–27.

Booth, B., J. Lewin, and C. J. Lorenzen (1988), Summer growth rates of subarctic Pacific phytoplankton assemblages determined from carbon uptake and cell volumes estimated using epifluorescence microscopy, *Mar. Biol.*, *98*, 287–298.

Booth, B. C., J. Lewin, and J. R. Postel (1993), Temporal variation in the structure of autotrophic and heterotrophic communities in the subarctic Pacific, *Prog. Oceanogr.*, *32*(1–4), 57–99.

Boyd, P., and P. J. Harrison (1999), Phytoplankton dynamics in the NE subarctic Pacific, *Deep Sea Res. Part II*, *46*(11–12), 2405–2432, doi:10.1016/S0967-0645(99)00069-7.

Boyd, P., and P. Newton (1995), Evidence of the potential influence of planktonic community structure on the interannual variability of particulate organic carbon flux, *Deep Sea Res. Part I*, *42*(5), 619–639, doi:10.1016/0967-0637(95)00017-Z.

Boyd, P. W., and P. P. Newton (1999), Does planktonic community structure determine downward particulate organic carbon flux in different oceanic provinces?, *Deep Sea Res. Part I*, *46*(1), 63–91, doi:10.1016/S0967-0637(98)00066-1.

Boyd, P., D. Muggli, D. Varela, R. Goldblatt, R. Chretien, K. Orians, and P. Harrison (1996), In vitro iron enrichment experiments in the NE subarctic Pacific, *Mar. Ecol. Prog. Ser.*, *136*, 179–193.

Boyd, P. W., et al. (2004), The decline and fate of an iron-induced subarctic phytoplankton bloom, *Nature*, *428*(6982), 549–53, doi:10.1038/nature02437.

Cassar, N., B. A. Barnett, M. L. Bender, J. Kaiser, R. C. Hamme, and B. Tilbrook (2009), Continuous high-frequency dissolved O_2/Ar measurements by equilibrator inlet mass spectrometry, *Anal. Chem.*, *81*(5), 1855–64, doi:10.1021/ac802300u.

Charette, M. A., S. B. Moran, and J. K. B. Bishop (1999), ^{234}Th as a tracer of particulate organic carbon export in the subarctic northeast Pacific Ocean, *Deep Sea Res. Part II*, *46*(11–12), 2833–2861, doi:10.1016/S0967-0645(99)00085-5.

Chen, C., and A. V. Borges (2009), Reconciling opposing views on carbon cycling in the coastal ocean: Continental shelves as sinks and near-shore ecosystems as sources of atmospheric CO_2, *Deep Sea Res. Part II*, *56*, 578–590.

Chierici, M., A. Fransson, and Y. Nojiri (2006), Biogeochemical processes as drivers of surface fCO_2 in contrasting provinces in the subarctic North Pacific Ocean, *Global Biogeochem. Cycles*, *20*(1), 1–16, doi:10.1029/2004GB002356.

Childers, A., T. Whitledge, and D. Stockwell (2005), Seasonal and interannual variability in the distribution of nutrients and chlorophyll a across the Gulf of Alaska shelf: 1998–2000, *Deep Sea Res. Part II*, *52*(1–2), 193–216, doi:10.1016/j.dsr2.2004.09.018.

Craig, H., and T. Hayward (1987), Oxygen supersaturation in the ocean: Biological versus physical contributions, *Science*, *235*(4785), 199–202.

Cunningham, A., D. McKee, S. Craig, G. Tarran, and C. Widdicombe (2003), Fine-scale variability in phytoplankton community structure and inherent optical properties measured from an autonomous underwater vehicle, *J. Mar. Syst.*, *43*(1–2), 51–59, doi:10.1016/S0924-7963(03)00088-5.

De Boyer Montégut, C., G. Madec, A. S. Fischer, A. Lazar, and D. Iudicone (2004), Mixed layer depth over the global ocean: An examination of profile data and a profile-based climatology, *J. Geophys. Res.*, *109*, C12003, doi:10.1029/2004JC002378.

Dunne, J. P., J. L. Sarmiento, and A. Gnanadesikan (2007), A synthesis of global particle export from the surface ocean and cycling through the ocean interior and on the seafloor, *Global Biogeochem. Cycles*, *21*(4), 1–16, doi:10.1029/2006GB002907.

Emerson, S. (1987), Seasonal oxygen cycles and biological new production in surface waters of the subarctic Pacific Ocean, *J. Geophys. Res.*, *92*(C6), 6535–6544.

Emerson, S., and C. Stump (2010), Net biological oxygen production in the ocean—II: Remote in situ measurements of O_2 and N_2 in subarctic pacific surface waters, *Deep Sea Res. Part I*, *57*(10), 1255–1265, doi:10.1016/j.dsr.2010.06.001.

Emerson, S., P. Quay, C. Stump, D. Wilbur, and M. Knox (1991), O_2, Ar, N_2 and ^{222}Rn in surface waters of the subarctic ocean: net biological O_2 production, *Global Biogeochem. Cycles*, *5*(1), 49–69.

Emerson, S., P. D. Quay, C. Stump, D. Wilbur, and R. Schudlich (1995), Chemical tracers of productivity and respiration in the subtropical Pacific Ocean, *J. Geophys. Res.*, *100*(C8), 15873–15887, doi:10.1029/95JC01333.

Fassbender, A. J., C. L. Sabine, R. A. Feely, C. Langdon, and C. W. Mordy (2011), Inorganic carbon dynamics during northern California coastal upwelling, *Cont. Shelf Res.*, *31*(11), 1180–1192, doi:10.1016/j.csr.2011.04.006.

Favorite, F., A. J. Dodimead, and K. Nasu (1976), *Oceanography of the Subarctic Pacific Region, 1960–1971*, Bulletin No. 33, 187 pp., International North Pacific Fisheries Commission, Vancouver, Canada.

Feely, R. A., R. Wanninkhof, H. B. Milburn, C. E. Cosca, and M. Stapp (1998), A new automated underway system for making high precision pCO_2 measurements onboard research ships, *Anal. Chim. Acta*, *377*(2–3), 185–191.

Francois, R., S. Honjo, R. Krishfield, and S. Manganini (2002), Factors controlling the flux of organic carbon to the bathypelagic zone of the ocean, *Global Biogeochem. Cycles*, *16*(4), doi:10.1029/2001GB001722.

Friedlingstein, P., R. A. Houghton, G. Marland, J. Hackler, T. A. Boden, T. J. Conway, J. G. Canadell, M. R. Raupach, P. Ciais, and C. Le Quéré (2010), Update on CO_2 emissions, *Nature Geosci.*, *3*(12), 811–812, doi:10.1038/ngeo1022.

Frost, B. W. (1993), A modelling study of processes regulating plankton standing stock and production in the open subarctic Pacific Ocean, *Prog. Oceanogr.*, *32*(1–4), 17–56, doi:10.1016/0079-6611(93)90008-2.

Garcia, H. E., and L. I. Gordon (1992), Oxygen solubility in seawater: Better fitting solubility equations, *Limnol. Oceanogr.*, *37*(6), 1307–1312.

Hales, B., T. Takahashi, and L. Bandstra (2005), Atmospheric CO_2 uptake by a coastal upwelling system, *Global Biogeochem. Cycles*, *19*(1), 1–11, doi:10.1029/2004GB002295.

Hamme, R., and S. Emerson (2004), The solubility of neon, nitrogen and argon in distilled water and seawater, *Deep Sea Res. Part I*, *51*(11), 1517–1528, doi:10.1016/j.dsr.2004.06.009.

Harrison, P., P. Boyd, D. Varela, S. Takeda, A. Shiomoto, and T. Odate (1999), Comparison of factors controlling phytoplankton productivity in the NE and NW subarctic Pacific gyres, *Prog. Oceanogr.*, *43*(2–4), 205–234.

Ho, D. T., C. S. Law, M. J. Smith, P. Schlosser, M. Harvey, and P. Hill (2006), Measurements of air-sea gas exchange at high wind speeds in the Southern Ocean: Implications for global parameterizations, *Geophys. Res. Lett.*, *33*, L16611, doi:10.1029/2006GL026817.

Johnson, W. K., L. A. Miller, N. E. Sutherland, and C. S. Wong (2005), Iron transport by mesoscale Haida eddies in the Gulf of Alaska, *Deep Sea Res. Part II*, *52*(7–8), 933–953, doi:10.1016/j.dsr2.2004.08.017.

Juranek, L. W., and P. D. Quay (2005), In vitro and in situ gross primary and net community production in the North Pacific Subtropical Gyre using labeled and natural abundance isotopes of dissolved O_2, *Global Biogeochem. Cycles*, *19*(3), doi:10.1029/2004GB002384.

Kahl, L., A. Vardi, and O. Schofield (2008), Effects of phytoplankton physiology on export flux, *Mar. Ecol. Prog. Ser.*, *354*, 3–19, doi:10.3354/meps07333.

Ladd, C., N. B. Kachel, C. W. Mordy, and P. J. Stabeno (2005), Observations from a Yakutat eddy in the northern Gulf of Alaska, *J. Geophys. Res.*, *110*, C03003, doi:10.1029/2004JC002710.

Laws, E. A. (1991), Photosynthetic quotients, new production and net community production in the open ocean, *Deep-Sea Res.*, *38*(1), 143–167.

Laws, E., P. Falkowski, W. J. Smith, H. Ducklow, and J. McCarthy (2000), Temperature effects on export production in the open ocean, *Global Biogeochem. Cycles*, *14*(4), 1231–1246.

Le Quéré, C., et al. (2009), Trends in the sources and sinks of carbon dioxide, *Nature Geosci.*, *2*(12), 831–836, doi:10.1038/ngeo689.

Lippiatt, S. M., M. C. Lohan, and K. W. Bruland (2010), The distribution of reactive iron in northern Gulf of Alaska coastal waters, *Mar. Chem.*, *121*(1–4), 187–199, doi:10.1016/j.marchem.2010.04.007.

Lippiatt, S. M., M. T. Brown, M. C. Lohan, and K. W. Bruland (2011), Reactive iron delivery to the Gulf of Alaska via a Kenai eddy, *Deep Sea Res. Part I*, *58*(11), 1091–1102, doi:10.1016/j.dsr.2011.08.005.

Liss, P. S., and L. Merlivat (1986), Air-sea gas exchange rates: Introduction and synthesis, in *The Role of Air-Sea Exchange in Geochemical Cycling*, edited by P. Buat-Menard, pp. 113–129, D. Reidel, Hingham, Mass.

Lorenzen, C. J. (1966), A method for the continuous measurement of in vivo chlorophyll concentration, in *Deep Sea Res.*, vol. 13, pp. 223–227, Elsevier.

Lutz, M. J., K. Caldeira, R. B. Dunbar, and M. J. Behrenfeld (2007), Seasonal rhythms of net primary production and particulate organic carbon flux to depth describe the efficiency of biological pump in the global ocean, *J. Geophys. Res.*, *112*, C10011, doi:10.1029/2006JC003706.

Marchetti, A., N. D. Sherry, H. Kiyosawa, A. Tsuda, and P. J. Harrison (2006), Phytoplankton processes during a mesoscale iron enrichment in the NE subarctic Pacific: Part I—Biomass and assemblage, *Deep Sea Res. Part II*, *53*(20–22), 2095–2113, doi:10.1016/j.dsr2.2006.05.038.

Marinov, I., M. Follows, A. Gnanadesikan, J. L. Sarmiento, and R. D. Slater (2008), How does ocean biology affect atmospheric pCO_2? Theory and models, *J. Geophys. Res.*, *113*, C07032, doi:10.1029/2007JC004598.

Martin, J. H., and S. E. Fitzwater (1988), Iron deficiency limits phytoplankton growth in the north-east Pacific subarctic, *Nature*, *331*, 341–343.

Montagnes, D. J. S., J. A. Berges, P. J. Harrison, and F. Taylor (1994), Estimating carbon, nitrogen, protein, and chlorophyll a from volume in marine phytoplankton, *Limnol. Oceanogr.*, *39*(5), 1044–1060.

Monterey, G., and S. Levitus (1997), Seasonal Variability of the Mixed Layer Depth for the World Ocean, *NOAA Atlas NESDIS*, *14*(5), 96 pp.

Mordy, C., P. Stabeno, C. Ladd, S. Zeeman, D. P. Wisegarver, S. A. Salo, and G. L. Hunt (2005), Nutrients and primary production along the eastern Aleutian Island Archipelago, *Fish. Oceanogr.*, *14*, 55–76.

Muller-Karger, F. E., R. Varela, R. Thunell, R. Luerssen, C. Hu, and J. J. Walsh (2005), The importance of continental margins in the global carbon cycle, *Geophys. Res. Lett.*, *32*, L01602, doi:10.1029/2004GL021346.

Murphy, P., Y. Nojiri, D. Harrison, and N. Larkin (2001), Scales of spatial variability for surface ocean pCO_2 in the Gulf of Alaska and Bering Sea: Toward a sampling strategy, *Geophys. Res. Lett.*, *28*(6), 1047–1050.

Napp, J. M., L. S. Incze, P. B. Ortner, D. L. W. Siefert, and L. Britt (1996), The plankton of Shelikof Strait, Alaska: standing stock, production, mesoscale variability and their relevance to larval fish survival, *Fish. Oceanogr.*, *5*(Suppl. 1), 19–38.

Nightingale, P. D., G. Malin, C. S. Law, A. J. Watson, P. S. Liss, M. I. Liddicoat, J. Boutin, and R. C. Upstill-Goddard (2000), In situ evaluation of air-sea gas exchange parameterizations using novel conservative and volatile tracers, *Global Biogeochem. Cycles*, *14*(1), 373–387.

Olson, R. J., E. R. Zettler, and O. K. Anderson (1989), Discrimination of eukaryotic phytoplankton cell types from light scatter and autofluorescence properties measured by flow cytometry, *Cytometry*, *10*(5), 636–43, doi:10.1002/cyto.990100520.

Peterson, T. D., D. W. Crawford, and P. J. Harrison (2011), Mixing and biological production at eddy margins in the eastern Gulf of Alaska, *Deep Sea Res. Part I*, *58*, 377–389, doi:10.1016/j.dsr.2011.01.010.

Pierrot, D., C. Neill, K. Sullivan, R. Castle, R. Wanninkhof, H. Luger, T. Johannessen, A. Olsen, R. A. Feely, and C. E. Cosca (2009), Recommendations for autonomous underway pCO_2 measuring systems and data-reduction routines, *Deep Sea Res. Part II*, *56*(8–10), 512–522, doi:10.1016/j.dsr2.2008.12.005.

Prokopenko, M. G., J. Granger, C. Mordy, N. Cassar, P. J. DiFiore, N. Kachel, D. Kachel, E. D. Cokelet, D. M. Sigman, and B. Moran (2010), Primary Production on the Eastern Bering Sea Shelf as Estimated from Oxygen/Argon Ratios and Triple Oxygen Isotopes, in *Proceedings from the 2010 AGU Ocean Sciences Meeting*.

Redfield, A. C., B. H. Ketchum, and F. A. Richards (1963), The influence of organisms on the composition of seawater, in *The sea*, edited by M. N. Hill, vol. 2, pp. 26–77, Interscience.

Reuer, M. K., B. A. Barnett, M. L. Bender, P. G. Falkowski, and M. B. Hendricks (2007), New estimates of Southern Ocean biological production rates from O_2/Ar ratios and the triple isotope composition of O_2, *Deep Sea Res. Part I*, *54*(6), 951–974, doi:10.1016/j.dsr.2007.02.007.

Ribalet, F., A. Marchetti, K. A. Hubbard, K. Brown, C. A. Durkin, R. Morales, M. Robert, J. E. Swalwell, P. D. Tortell, and E. V. Armbrust (2010), Unveiling a phytoplankton hotspot at a narrow boundary between coastal and offshore waters, *Proc. Nat. Acad. Sci. U.S.A.*, *107*(38), 16571–6, doi:10.1073/pnas.1005638107.

Ribalet, F., D. M. Schruth, and E. V. Armbrust (2011), flowPhyto: enabling automated analysis of microscopic algae from continuous flow cytometric data, *Bioinformatics*, *27*(5), 732–3, doi:10.1093/bioinformatics/btr003.

Richardson, T. L., and G. A. Jackson (2007), Small phytoplankton and carbon export from the surface ocean, *Science*, *315*(5813), 838–40, doi:10.1126/science.1133471.

Signorini, S. R., C. R. McClain, J. R. Christian, and C. Wong (2001), Seasonal and interannual variability of phytoplankton, nutrients, TCO_2, pCO_2, and O_2 in the eastern subarctic Pacific (ocean weather station Papa), *J. Geophys. Res.*, *106*(C12), 31197–31215.

Smayda, T. J. (1970), The suspension and sinking of phytoplankton in the sea, *Oceanogr. Mar. Biol. Ann. Rev.*, *8*, 353–414.

Sosik, H. M., S. W. Chisholm, and R. J. Olson (1989), Chlorophyll fluorescence from single cells: Interpretation of flow cytometric signals, *Limnol. Oceanogr.*, *34*(8), 1749–61.

Stabeno, P. J., N. A. Bond, A. J. Hermann, N. B. Kachel, C. W. Mordy, and J. E. Overland (2004), Meteorology and oceanography of the Northern Gulf of Alaska, *Cont. Shelf Res.*, *24*(7–8), 859–897, doi:10.1016/j.csr.2004.02.007.

Stanley, R. H. R., J. B. Kirkpatrick, N. Cassar, B. A. Barnett, and M. L. Bender (2010), Net community production and gross primary production rates in the western equatorial Pacific, *Global Biogeochem. Cycles*, *24*(4), 1–17, doi:10.1029/2009GB003651.

Strom, S., M. Olson, E. Macri, and C. Mordy (2006), Cross-shelf gradients in phytoplankton community structure, nutrient utilization, and growth rate in the coastal Gulf of Alaska, *Mar. Ecol. Prog. Ser.*, *328*, 75–92.

Stukel, M. R., M. R. Landry, C. R. Benitez-Nelson, and R. Goericke (2011), Trophic cycling and carbon export relationships in the California Current Ecosystem, *Limnol. Oceanogr.*, *56*(5), 1866–1878, doi:10.4319/lo.2011.56.5.1866.

Suga, T., K. Motoki, Y. Aoki, and A. M. Macdonald (2004), The North Pacific climatology of winter mixed layer and mode waters, *J. Phys. Oceanogr.*, *34*(1), 3–22, doi:10.1175/1520-0485(2004)034<0003:TNPCOW>2.0.CO;2.

Suzuki, K., H. Liu, T. Saino, H. Obata, M. Takano, K. Okamura, Y. Sohrin, and Y. Fujishima (2002), East–west gradients in the photosynthetic potential of phytoplankton and iron concentration in the subarctic Pacific Ocean during early summer, *Limnol. Oceanogr.*, *47*(6), 1581–1594, doi:10.4319/lo.2002.47.6.1581.

Swalwell, J. E., F. Ribalet, and E. V. Armbrust (2011), SeaFlow: A novel underway flow-cytometer for continuous observations of phytoplankton in the ocean, *Limnol. Oceanogr.: Methods*, *9*, 466–477, doi:10.4319/lom.2011.9.466.

Sweeney, C., E. Gloor, A. R. Jacobson, R. M. Key, G. McKinley, J. L. Sarmiento, and R. Wanninkhof (2007), Constraining global air-sea gas exchange for CO_2 with recent bomb ^{14}C measurements, *Global Biogeochem. Cycles*, *21*(2), 1–10, doi:10.1029/2006GB002784.

Takahashi, T., et al. (2002), Global sea-air CO_2 flux based on climatological surface ocean pCO_2, and seasonal biological and temperature effects, *Deep Sea Res. Part II*, *49*(9–10), 1601–1622.

Takahashi, T., et al. (2009), Climatological mean and decadal change in surface ocean pCO_2, and net sea-air CO_2 flux over the global oceans, *Deep Sea Res. Part II*, *56*(8–10), 554–577, doi:10.1016/j.dsr2.2008.12.009.

Thomson, R. E., and I. V. Fine (2003), Estimating mixed layer depth from oceanic profile data, *J. Atmos. Oceanic Tech.*, *20*(2), 319–329.

Thyssen, M., N. Garcia, and M. Denis (2009), Sub meso scale phytoplankton distribution in the North East Atlantic surface waters determined with an automated flow cytometer, *Biogeosciences*, *6*(4), 569–583, doi:10.5194/bg-6-569-2009.

Tortell, P. D. (2005), Dissolved gas measurements in oceanic waters made by membrane inlet mass spectrometry, *Limnol. Oceanogr.: Methods*, *3*, 24–37.

Tsuda, A., et al. (2003), A mesoscale iron enrichment in the western subarctic Pacific induces a large centric diatom bloom, *Science*, *300*(5621), 958–61, doi:10.1126/science.1082000.

Verity, P. G., C. Y. Robertson, C. R. Tronzo, M. G. Andrews, J. R. Nelson, and M. E. Sieracki (1992), Relationships between cell volume and the carbon and nitrogen content of marine photosynthetic nanoplankton, *Limnol. Oceanogr.*, *37*(7), 1434–1446, doi:10.4319/lo.1992.37.7.1434.

Volk, T., and M. I. Hoffert (1985), Ocean Carbon Pumps: Analysis of relative strengths and efficiencies in ocean-driven atmospheric CO_2 changes, in *The Carbon Cycle and Atmospheric CO_2 Natural Variations Archean to Present*, edited by E. T. Sundquist, and W. S. Broecker, vol. 32, pp. 99–110, American Geophysical Union, Wahington, DC.

Wanninkhof, R. (1992), Relationship between wind speed and gas exchange over the ocean, *J. Geophys. Res.*, *97*(C5), 7373–7382.

Weiss, R. (1974), Carbon dioxide in water and seawater: the solubility of a non-ideal gas, *Mar. Chem.*, *2*(3), 203–215.

Westberry, T., M. J. Behrenfeld, D. A. Siegel, and E. Boss (2008), Carbon-based primary productivity modeling with vertically resolved photoacclimation, *Global Biogeochem. Cycles*, *22*(2), 1–18, doi:10.1029/2007GB003078.

Wheeler, P. A. (1993), New production in the subarctic Pacific Ocean: Net changes in nitrate concentrations, rates of nitrate assimilation and accumulation of particulate nitrogen, *Prog. Oceanogr.*, *32*(1–4), 137–161, doi:10.1016/0079-6611(93)90011-2.

Whitney, F. A., W. R. Crawford, and P. J. Harrison (2005), Physical processes that enhance nutrient transport and primary productivity in the coastal and open ocean of the subarctic NE Pacific, *Deep Sea Res. Part II*, *52*(5–6), 681–706, doi:10.1016/j.dsr2.2004.12.023.

Wise, D. L., and G. Houghton (1966), The diffusion coefficients of ten slightly soluble gases in water at 10-60°C, *Chem. Eng. Sci.*, *21*, 999–1010.

Wong, C., and Y. H. Chan (1991), Temporal variations in the partial pressure and flux of CO_2 at ocean station P in the subarctic northeast Pacific Ocean, *Tellus*, *43B*(2), 206–223.

Wong, C. S., N. A. D. Waser, Y. Nojiri, F. A. Whitney, J. S. Page, and J. Zeng (2002), Seasonal cycles of nutrients and dissolved inorganic carbon at high and mid latitudes in the North Pacific Ocean during the Skaugran cruises: determination of new production and nutrient uptake ratios, *Deep Sea Res., Part II*, *49*, 5317–5338.

Wu, J., A. Aguilar-Islas, R. Rember, T. Weingartner, S. Danielson, and T. Whitledge (2009), Size-fractionated iron distribution on the northern Gulf of Alaska, *Geophys. Res. Lett.*, *36*, L11606, doi:10.1029/2009GL038304.

Zeng, J., Y. Nojiri, P. P. Murphy, C. S. Wong, and Y. Fujinuma (2002), A comparison of ΔpCO_2 distributions in the northern North Pacific using results from a commercial vessel in 1995–1999, *Deep Sea Res., Part II*, *49*, 5303–5315.